DOI 10.1007/s11106-022-00298-6
Powder Metallurgy and Metal Ceramics, Vol. 61, Nos. 1-2, May, 2022 (Russian Original Vol. 61, Nos. 1-2, Jan.-Feb., 2022)

THE EFFECT OF STRONTIUM CONTENT ON THE CORROSION BEHAVIOR OF NEW BIODEGRADABLE Mg–1Ca–1Y COMPOSITE FOR IMPLANT APPLICATION

Mustafa Özgür Öteyaka,[1,4] Fatih Apaydin,[2] and Şule Apaydin[3]

UDC 669.892;669.721

In this study, new biodegradable magnesium composites Mg–1Ca–1Y–xSr (x = 0.5, 1.0, 1.5, and 2.0) were designed and produced by mechanical alloying to improve the corrosion properties. X-ray diffraction (XRD) and field-emission scanning electron microscopy (FE-SEM) were employed to characterize the resulting biodegradable magnesium composites. Besides, the corrosion process was monitored with the help of electrochemical corrosion testing methods, such as open circuit potential (OCP), anodic polarization, and electrochemical impedance spectroscopy (EIS). The results showed that the microstructure of the composites consisted of different phases, with their amounts increasing when adding Sr. Moreover, the phase analysis revealed the formation of intermetallic phases Mg_2Ca, $Mg_{17}Sr_2$, *and* $Mg_{24}Y_5$ *in the composites. The immersion of composites in 0.9 wt.% NaCl solution exhibited cathodic potential after 2 h. Enhanced corrosion potential was obtained for a 2.0 wt.% Sr composite. In contrast, composite A with the lowest Sr content exhibited higher cathodic corrosion potential. Analysis of the anodic curves revealed passivation behavior for all composites after immersion into the solution. In addition, pitting was observed on the sample's surface, and the potential for pitting increased for the Mg–1Ca–1Y composite. On the other hand, a semi-circle capacitive loop was noted for all composites, and polarization resistance of the film was better for Mg–1Ca–1Y–2Sr than other samples. That is probably due to the involvement of Sr in the protective oxide layer and the decrease of the galvanic effect in the microstructure. In general, the addition of Sr was favorable for the new biodegradable Mg–1Ca–1Y composite, which may be considered a promising candidate for biodegradable magnesium implants.*

Keywords: *Mg–Ca–Y–Sr composite, corrosion, biodegradable, mechanical alloying, magnesium.*

INTRODUCTION

Magnesium and its alloys have recently gained academic interest in manufacturing new biodegradable materials. Recent research works showed that magnesium alloys could be used as biodegradable implants in orthopedic operations instead of current metallic biomaterials due to the lower elastic modulus (41–45 GPa) [1–4]. The disadvantage of such currently used metallic biomaterials as Ti6Al4V, 316L, and Co–Cr–Mo alloys is their high elastic modulus (>60 GPa) [5].

[1] Eskisehir Osmangazi University, Eskisehir Vocational School, Department of Electronic and Automation, Eskisehir, Turkey. [2] Bilecik Şeyh Edebali University, Engineering Faculty, Department of Metallurgy and Materials, Bilecik, Turkey. [3] Turkey Rail Vehicle Industry System Joint Stock Company (TÜRASAŞ), Eskisehir, Turkey.

[4] To whom correspondence should be addressed; e-mail: moteyaka@ogu.edu.tr.

Published in Poroshkova Metallurgiya, Vol. 61, Nos. 1–2 (543), pp. 128–141, 2022. Original article submitted September 29, 2020.

Magnesium biodegradable materials meet the above criteria and are classified as metal implants because it is already present in the human biological system (approximately 121 mg/L in the blood) [2, 3, 6, 7]. However, using only unalloyed Mg may not guarantee the slow degradation and good mechanical properties required for orthopedic application. On the other hand, conventional Mg alloys from AZ groups were found to have higher cytotoxicity causing genotoxicity due to the presence of Al and Zn [6]. For this reason, the strategy of developing magnesium biodegradable materials was alloying with non-toxic elements like Ca, Sr, and rare earth elements (REEs) [7–13]. It is well known that both Ca and Sr are essential biodegradable elements involved in bone formation [4, 9, 14, 15]. Depending on the quantity of Ca, the corrosion resistance and mechanical properties of Mg and its alloys may vary, as mentioned in literature [12, 16–21]. The addition of Ca in Mg generates Mg_2Ca phases that precipitate throughout the grain boundaries [22] and act as anodic sites in the microstructure [23].

Different quantities of Ca were studied to analyze the corrosion performance of Mg–Ca alloy. Thus, Mohamed et al. [24] showed that the Mg–0.8Ca alloy had a higher degradation rate compared to pure Mg. The pitting potential of the Mg–0.8Ca alloy was –1.72 V in Hank's balanced salt solution (HBSS), which is –0.13 V more cathodic than pure Mg. Furthermore, it was reported that increasing the content of Ca from 0.5 to 2.0 wt.% facilitated the corrosion of Mg–xCa in simulated body fluid (SBF) [22]. Also, Sr participates in grain refinement of Mg, enhancing thus its mechanical properties [14].

The effect of Sr on the corrosion of biodegradable magnesium alloy with different compositions of Mg and other elements was studied [5, 9, 25]. For example, Li et al. [5] examined the corrosion performance of Mg–Zr–Sr alloys as biodegradable implants in SBF and cell culture medium (CCM). Measurements of open-circuit potential (OCP) and corrosion rate revealed that the alloy containing 2.0 and 5.0% Sr exhibited better corrosion performance in CCM than SBF. The OCP for Mg2Zr2Sr and Mg5Zr5Sr were similar in the cell culture medium, and the E_{corr} amounted to approximately –1.6 V. The role of strontium in amount of 0.2–1.0 wt.% in the Mg–2Zn–2Ca–0.5Mn (ZXM220) cast was evaluated for potential implant application [9]. The corrosion rate of ZXM220–0.2Sr was 0.68 mm/year lower than of analogs. Besides, increasing Sr content up to 1.0 wt.% in the cast alloy shifted the pitting potential of 0.01 V towards negative values compared to Mg–2Zn–2Ca–0.5Mn (ZXM220). Similar works demonstrated that adding 0.2 wt.% Sr in various Mg alloys like Mg–2Zn–0.2Sr [26], Mg–5Zn–0.2Sr [27], and Mg–1Zn–1Mn–0.25Sr [28] improved the corrosion resistance.

Also, the addition of yttrium increased the strength and corrosion resistance of Mg [29–31]. Different authors investigated the influence of Y on the corrosion of Mg in various media. Thus, Zucci et al. [32] measured the corrosion of Mg alloy WE43 containing 3.92% Y and 2.09% Nd in sulfate and chloride medium. The dissolution rate was higher in chloride than in sulfate medium due to galvanic corrosion. Thus, the $E_{\text{corr}} = -1.75$ V/SCE in chloride medium versus –1.71 V/SCE in sulphate medium after 1 h of immersion. According to Li et al. [22], the addition of Y in amount of 1 wt.% to the Mg–1Ca alloy in SBF increased the corrosion rate. Although the corrosion properties of biodegradable magnesium alloy were greatly affected by the elements, the production methods also influence the corrosion behavior of the biodegradable materials. Hence, Mg and its alloys/composites are characterized by a high level of degradation in body fluid, which is a significant problem. On the other hand, they are one of the most promising materials for implants because of their biocompatibility.

The objective of this study is to enhance the corrosion properties of the newly developed biodegradable Mg–1Ca–1Y composites by adding different amounts of Sr. According to some authors, Sr had a beneficial effect on the corrosion resistance of Mg [5, 9, 25]. The new magnesium composite contained Ca and Y, which remained consistent in the alloy and are biocompatible. Besides, Sr in the content of 0.5–2.0 wt.% was added to Mg–1Ca–1Y composite through mechanical alloying and sintering. The corrosion performance of the composite was evaluated by open circuit potential, anodic polarization (AP), and electrochemical impedance spectroscopy (EIS) in 0.9 wt.% isotonic solution.

MATERIALS AND METHODS

Materials Preparation. Magnesium (Mg), calcium (Ca), yttrium (Y), and strontium (Sr) powders were obtained from Sigma Aldrich and were used in this study as raw materials for preparing samples. A total of five samples were prepared by mechanical alloying. The respective chemical composition of the composite is provided

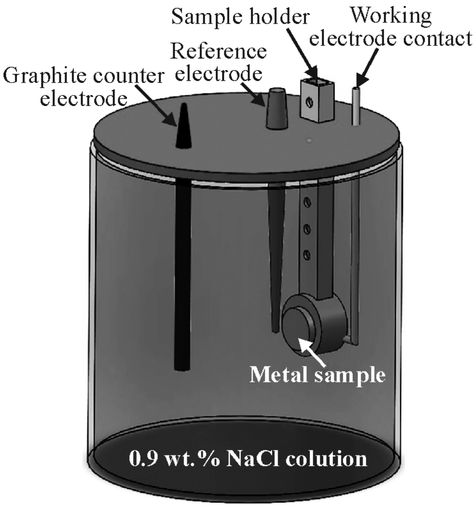

Fig. 1. Schematic presentation of a standard three-electrode cell

TABLE 1. The Chemical Composition of the Experimental Magnesium Composites

Code	Sample	Alloying elements, wt.%			
		Mg	Ca	Y	Sr
Reference	Mg1Ca1Y	Bal.	1	1	–
Composite A	Mg1Ca1Y0.5Sr	Bal.	1	1	0.5
Composite B	Mg1Ca1Y1Sr	Bal.	1	1	1
Composite C	Mg1Ca1Y1.5Sr	Bal.	1	1	1.5
Composite D	Mg1Ca1Y2Sr	Bal.	1	1	2

in Table 1. Besides, each composite was assigned a specific code to simplify identification and avoid confusion. Magnesium was used as a matrix, while the other raw materials served as alloying elements. A glove box was used to weigh powders. Afterward, powders were loaded into a steel vial to avoid powder oxidation. For this purpose, a vial and balls (10 mm in diameter) made of hardened stainless steel were employed. The ball-to-powder ratio was fixed at 10 : 1. The mixed fine grains were milled in dry conditions under an Ar atmosphere with a planetary ball press Fritsch-Pulverisette-5. The mechanical milling was accomplished at room temperature for 30 h (with a period of 10 min for each 30 min) at a rotational speed of 400 rpm. The milled compositions were then pressed on a 200 MPa manual hydraulic press, forming green compacts with a diameter of 13 mm. Subsequently, the samples were mounted in the tube furnace and sintered for 1 h under an Ar atmosphere at 550°C (heating and cooling velocity were 5 °C/min).

Electrochemical Test. The corrosion tests were performed using Gamry Interface 1000 potentiostat, and the results collected were evaluated using Gamry Echem Analyst tools. A three-electrode system, consisting of a working electrode, counter electrode, and reference electrode, was employed to test the magnesium composite's corrosion performance (Fig. 1). A 0.9 wt.% isotonic solution, also referred to as physiological saline solution, served as the corrosion environment. This solution was purchased from a drugstore. The working electrodes were connected with copper wire using copper tape. Then, the composite was mounted with cold epoxy resin. The working electrode had been ground with a 1200-grit grinding paper and cleaned with distilled water before each test. 1 cm^2 of the working electrode's surface was submerged with a reference electrode (silver/silver chloride (Ag/AgCl)) and a graphite rod as the counter electrode in 1 L of isotonic serum at room temperature. The sample was retained in the solution for 15 min before the test was initiated.

The electrochemical polarization techniques such as OCP, AP, and EIS were applied to the composites. The OCP or open voltage was recorded every 5 s for 2 h. Then, E_{corr} (V) vs. time (h) plots were drawn to analyze the electrochemical corrosion behavior of each composite in the solution. Meanwhile, the potentiodynamic curves were mapped between –2 V and +2 V at a scanning rate of 0.5 mV/s. Then, the data for E_{corr}, E_{pit}, and i_{corr} were evaluated from the potentiodynamic plots. The EIS measurement was performed with a voltage perturbation amplitude of 10 mV at a frequency range of 100 kHz to 0.01 Hz in potentiostatic EIS mode. Afterward, the Nyquist plots were traced to analyze the resistance of composites. Moreover, the electrical circuit was fitted to Nyquist plots using Gamry Echem Analyst software.

Surface Analysis. The surface of the composites was investigated using Hitachi Regulus 8230 model field-emission scanning electron microscopy (FE-SEM) with a backscattered electron detector (BSD). Furthermore, the energy dispersive spectrometry (EDS) was applied to identify the intermetallic phase in the microstructure of the composites. Each sample's X-Ray pattern was generated using an X-ray diffractometer (XRD) by Panalytical Empyrean with a scanning speed of 2° $\min^{-1}$ in the range of 0° to 90°. ImageJ free software was used to define the distribution of intermetallic phases for each composite. For this purpose, SEM images were converted to 8-bit, and the picture was modified using a "threshold" where the dark-grey phases (intermetallics) were painted red. The option "analyze particle" was selected from the options menu to display the count of phases.

RESULTS AND DISCUSSION

Composite Microstructure Analysis. The XRD analysis of the composites was performed to identify the phases. According to the results, the main peaks of Mg in the reference composite without Sr were located at 33°, 35°, and 38° (Fig. 2).

Moreover, the $Mg_{24}Y_2$ and Mg_2Ca intermetallics were observed at 29° and 31° on the XRD patterns. The addition of Sr in the reference composite facilitated the formation of a new intermetallic $Mg_{17}Sr_2$ phase located at 26° and 49°. On the other hand, the addition of Sr shifted peaks and increased their intensity. The findings on the location of intermetallic peaks complemented the data available in the literature [16, 22, 33, 34].

The influence of mechanical alloying on magnesium composites and the effect of the Sr amounts were investigated using FE-SEM imaging. Figure 3 presents the microstructure of composites. It can be seen that the surface of the composite contained different phases and some pores. A deeper analysis of the samples' distribution of phases was performed using energy-dispersive X-ray spectroscopy (EDX). The magnification of samples using the backscattering mode of FE-SEM revealed the distribution of a white phase throughout the microstructure of all samples (Fig. 3). The EDX analysis of this phase revealed the presence of a higher amount of yttrium element in composite C compared to composites A, B, and D, indicating the formation of the $Mg_{24}Y_5$ intermetallic phase, as found above (point 2 in Fig. 3, Table 2). However, some aggregation was observed in the composite A.

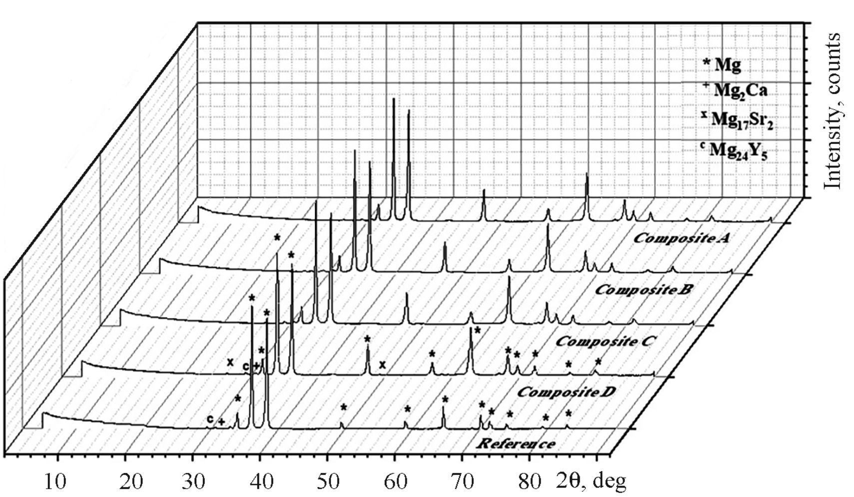

Fig. 2. The XRD pattern of the composites

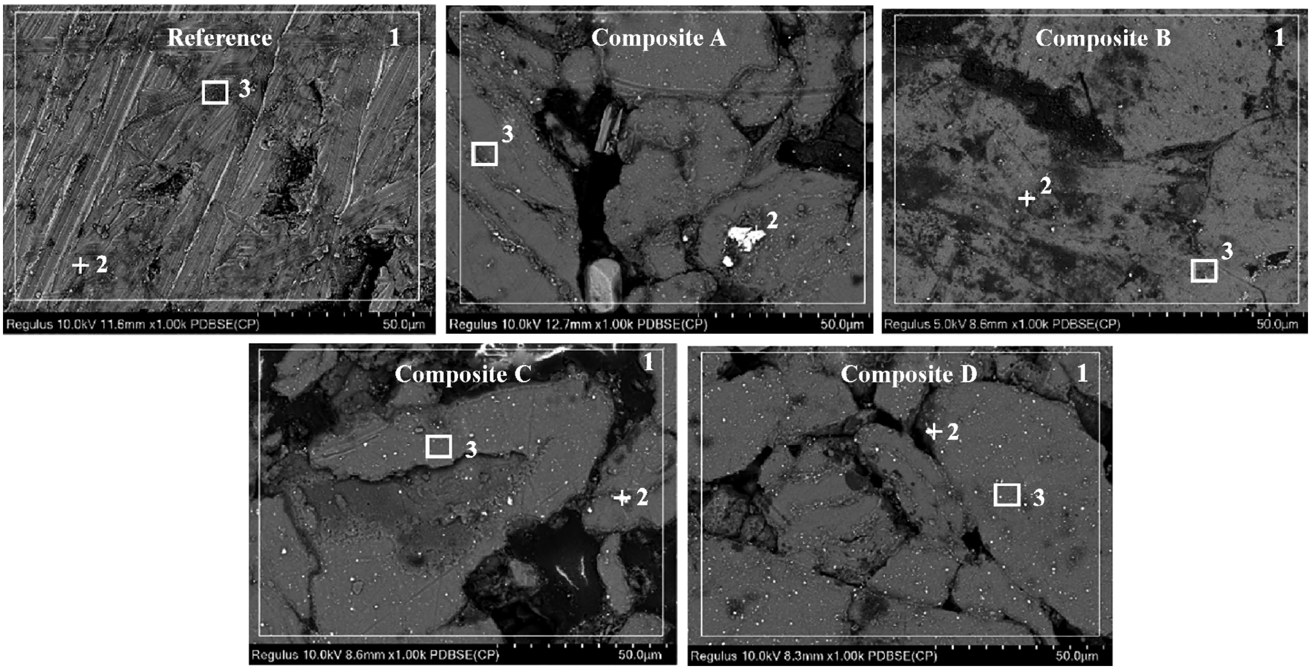

Fig. 3. FE-SEM images with EDS analysis point/area of magnesium composites

---

TABLE 3. The EDS Analysis Results of Composites from Fig. 3

Sample	*EDS No.	Element, wt.%					
		C	O	Mg	Ca	Sr	Y
Reference	1	17.00	14.45	67.00	0.80	–	0.75
	2	8.79	13.12	6.74	1.10	–	70.25
	3	9.52	14.25	77.23	0.90	–	0.30
Composite A	1	17.38	15.47	65.54	1.1	0.19	0.32
	2	9.26	19.83	9.81	1.1	0.3	59.7
	3	6.38	11.56	80.26	1.04	0.21	0.55
Composite B	1	18.4	9.14	70.1	0.82	0.74	0.80
	2	17.52	8.76	9.25	1.14	0.52	62.81
	3	10.64	4.82	83.33	0.29	0.1	0.82
Composite C	1	31.61	13.87	53.42	0.70	0.23	0.17
	2	9.56	3.20	0.97	0.05	0.48	85.74
	3	6.82	4.12	88.03	0.26	0.31	0.46
Composite D	1	15.66	14.64	67.32	1.31	0.44	0.63
	2	23.07	7.96	7.89	0.47	0.08	60.53
	3	8.30	6.40	83.7	0.75	0.26	0.59

*EDS number corresponds to the area or spot analysis: number 1—general area, number 2— white phase, and number 3—dark grey phase.

In general, the quantity of the Y element in the white phase (point 2) was higher for all composites than other elements. On the other hand, the analysis of the grey phase (square 3 in Fig. 3) showed the presence of magnesium elements with calcium, strontium, and yttrium, as expected. However, carbon and oxygen were also identified after milling (Table 2). The EDS analysis suggests that the microstructure most likely consisted of such

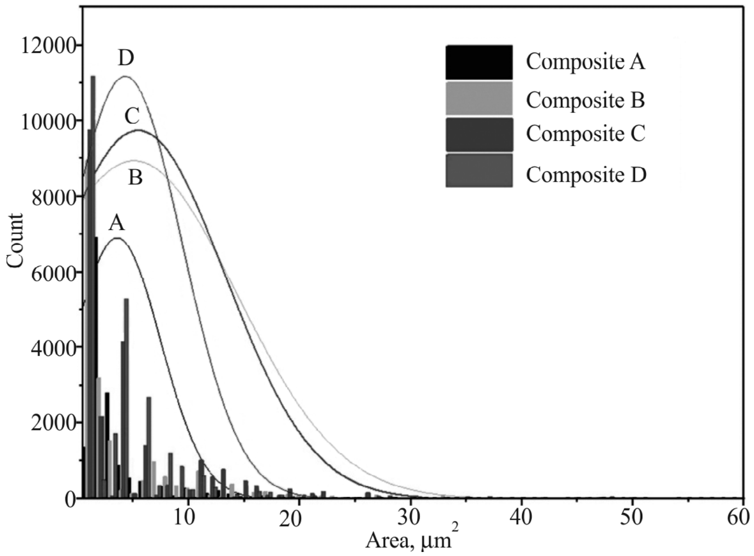

Fig. 4. The histogram with distribution curve of dark grey phase in the composites

intermetallic phases as Mg_2Ca (dark grey area), $Mg_{17}Sr_2$ (dark grey area), and $Mg_{24}Y_2$ (white area). Moreover, the white phase contained a Y element, suggesting that it mostly held the $Mg_{24}Y_2$ intermetallic phase. The distribution of the intermetallic phase in the matrix was dendritic in some areas.

Conversely, a random distribution of intermetallics was also noticed in the composites, which can benefit corrosion potential [25]. However, some porosity was observed in the microstructure of composites due to mechanical alloying. At the same time, such porous sites can be beneficial for the adhesion and proliferation of the cells, offering better compatibility for an implant.

The effect of the Sr content in the microstructure was also considered by analyzing the dark grey area of the phase (Fig. 4). From the phase distribution, it is evident that its presence increased simultaneously with the amount of Sr. In this respect, the lowest intermetallic phase formation was observed in composite A, while the highest was recorded for composite D. While increasing the intermetallic phase may improve the mechanical properties of the composite, corrosion properties may be negatively affected due to increased galvanic activity for some intermetallics. Evidently, the composites with moderate porosity were successfully fabricated. Furthermore, the addition of Sr increased the amount of intermetallic phase.

Corrosion Performance of the Composites. Free Corrosion Potential Behavior. It is known that when the surface of Mg is in contact with the chloride ion, an aggressive attack of the latter is observed, leading to pitting corrosion with $Mg(OH)_2$ products on the surface [20, 21, 35–37]. In this study, the corrosion potential of the

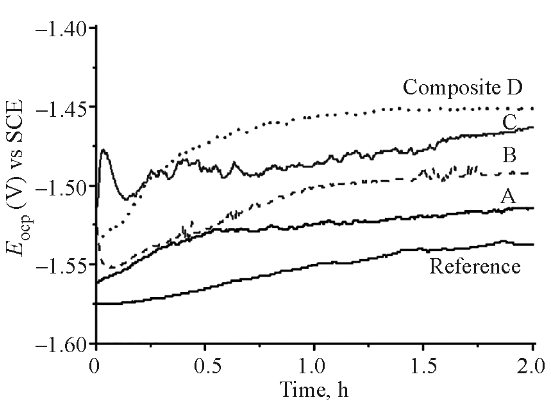

Fig. 5. The free corrosion potential measurement of the composites A–D in the 0.9 wt.% isotonic solutions over 2 h

composite was first measured by OCP to understand the behavior of the composite in the 0.9 wt.% isotonic solution. The open voltage of composites was presented in Fig. 5. The E_{corr} begins at the negative/cathodic value for all scans, rising immediately to a more positive/anodic direction within 2 h. During the E_{corr} measurement, some highs and lows of specific peaks were observed in the composite, which can be attributed to the activation/repassivation of the pits [20, 38]. The reference sample without Sr started at –1.57 V and increased toward the anodic direction during the experiment, ending at –1.54 V. The composite D with the highest Sr content had an E_{corr} value of –1.45 V at the end of 2 h in the 0.9 wt.% isotonic solutions. Decreasing the content of Sr from 2.0 to 0.5 wt.% in the composite shifted the E_{corr} towards negative values, indicating the reduction at the working electrode. The E_{corr} of composites A, B, and C completed the experiment with the values of –1.51, –1.49, and –1.46 V, respectively, indicating higher activity compared to the composite D. As such, it can be stated that adding and increasing the amount of Sr element in the Mg–1Ca–1Y composite was beneficial to corrosion resistance. This can be explained by both effects of Sr in the composite. Firstly, it increases SrO participating in the protective oxide layer. Secondly, the galvanic effect decreases due to a higher quantity of $Mg_{17}Sr_2$ in the microstructure that acts as a corrosion barrier.

Passivation Behavior of the Composite. The potentiodynamic technique was used to observe the aptitude of the metal in forming a protective film in the solution. Figure 6 represents the potentiodynamic plots of composites A–D. The corrosion potential (E_{corr}) and corrosion current densities (i_{corr}) were calculated using Tafel method, and the measurement data are provided in Table 3. According to the anodic curves, passivation zone was noted for all samples. The reference sample exhibited an E_{corr} value of –1.41 V, which is more cathodic than other samples. The curves show that the composite values did not vary significantly except for composite D, for which the E_{corr} shifted towards a positive direction. This difference can be explained by an increased amount of Sr in the composite D, as

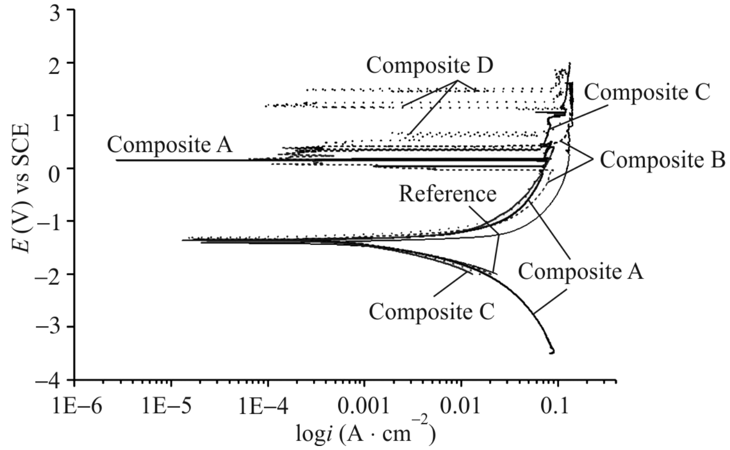

Fig. 6. Potentiodynamic curves of the composites A–D scanned at a rate of 0.5 mV/s in the 0.9 wt.% isotonic solution

TABLE 3. The Tafel Results of Composites Obtained from Potentiodynamic Curves in Fig. 6

Sample	β_a,V/decade	β_c, V/decade	i_{corr}, $\mu A \cdot cm^{-2}$	E_{corr}, V	E_{pit}, V
Reference	$106.7 \cdot 10^{-3}$	$433.0 \cdot 10^{-3}$	1240.0	–1.41	0.79
Composite A	$245.0 \cdot 10^{-3}$	$657.3 \cdot 10^{-3}$	1850.0	–1.36	0.05
Composite B	$169.1 \cdot 10^{-3}$	$396.3 \cdot 10^{-3}$	822.0	–1.35	–0.07
Composite C	$155.7 \cdot 10^{-3}$	$510.4 \cdot 10^{-3}$	947.0	–1.36	0.41
Composite D	$161.3 \cdot 10^{-3}$	$429.6 \cdot 10^{-3}$	589.0	–1.31	0.42

discussed above, since the Sr element contributes to the resistance of the protective oxide film on the composite. On the other hand, the analysis of anodic curves showed that composite. A exhibited two passivation zones located between (+0.05 V)–(+0.06 V) and (+0.16 V)–(+0.18 V). It should be noted that the formation of the protective film is an important indicator of the oxide film's resistance to the dissolution. The oxides engaged in forming a protective film for the composites A–D probably were MgO, CaO, Y_2O_3, and SrO [7, 14, 23].

Meanwhile, increasing the content of Sr to 1.0 wt.% induced the passivation zone to positive values with a higher interval area. The passivation zone was spotted between –0.07 V and +0.41 V for composite B. As expected, the passivation zone of composite C was also higher than that of composite B, located between +0.41 V and +1.10 V. Similar observation was true for composite D. However, three passivation zones were observed here instead of one. Thus, one was noted at around +0.42 V and +0.68 V, the second one between +1.16 V and +1.25 V, and the last at approximately +1.46 V and +1.51 V.

Hence, the pitting corrosion is localized corrosion occurring in magnesium alloys in the presence of Cl$^-$ ions [20, 35, 38]. Öteyaka et al. cited that the pits grow and passivate with the corrosion product that form a passivation zone in the potentiodynamic curves [20]. The critical pitting potential (E_{pit}) was also observed for composites during the anodic scanning in the isotonic solution. This potential is equal to the starting potential of the passivation zone. The E_{pit} was calculated for each composite; the calculations are presented in Table 3. The findings show that E_{pit} value of the reference sample was higher than the composite with 0.79 V, which means that pits are formed instead in the anodic zone. Besides, composites A (+0.05 V) and B (–0.07 V) were more negative compared to composites C (+0.41 V) and D (+0.42 V). The findings allow deducting that the addition of Sr in low amounts shifted the E_{pit} to a negative value, which is compatible with other results in the literature [36]. Additionally, the i_{corr} as a reference to electron flow from anode to cathode is a good indicator of corrosion activity. It was noticed that this electron transfer was more intense for composite A, followed by a reference composite, composite C, and composite D. As seen, adding up to 2 wt.% of Sr decreased the corrosion rate. This finding is consistent with the study by Li et al. [5], who also confirmed that the addition of Sr in an amount of below 2 wt. % significantly facilitated the degradation of Mg–Zr–Sr alloy (Table 3). Overall, composite D demonstrated a more pronounced passivation behavior with more anodic potential than its alternatives. As such, adding Sr element to the magnesium composite Mg–1Ca–1Y significantly affects the corrosion resistance in an isotonic solution.

Corrosion Resistance of the Composites. The electrochemical impedance is a non-destructive method used to determine the kinetic reaction between metal and solution. It allows a more precise analysis of the electron transfer resistance between the working electrode and solution. The results of EIS were presented as Nyquist plots in Fig. 7. Each composite exhibited a semi-circle capacitive loop at a high frequency attributed to the resistance interface between the isotonic solution and composite film. Such corrosion process at high frequency also means the relaxation of electrochemical reaction. Admittedly, a larger diameter of Nyquist curves represents better corrosion resistance [9]. Addition of Sr to Mg–1Ca–1Y composite gradually increased the semi-circle capacitive loop. It was observed that the diameter of the semi-circle increases with the quantity of Sr, implying a deceleration of the

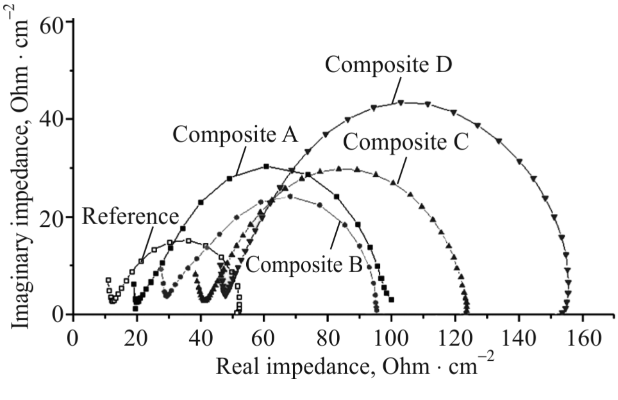

Fig. 7. Nyquist plots of the composites

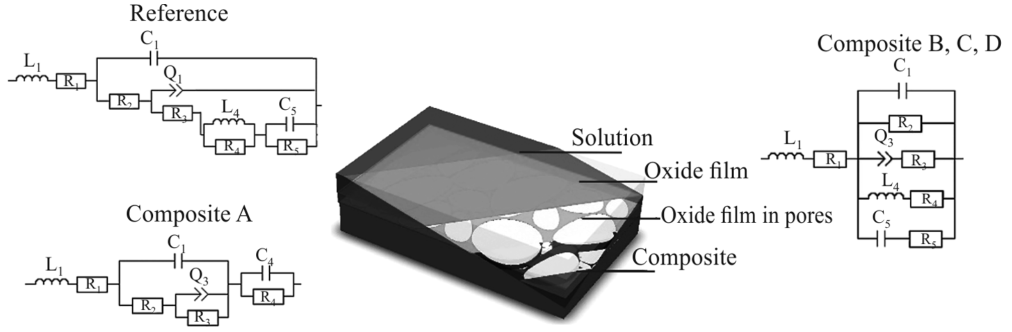

Fig. 8. The electrical equivalent circuit of the composites and diagonal cross-section view of the layers after immersion in the 0.9 wt.% isotonic solution

corrosion rate. According to these results, composite D demonstrated a better corrosion resistance than the other composites examined in this research.

Furthermore, inductive loop behavior indicating the adsorption of $Mg(OH)_2$ [32] was seen at low frequency for composites B, C, and D. The formation of an inductive loop can be possibly related to pit blockage [39]. The polarization resistance of each composite was calculated according to Nyquist plots, amounting to 52, 99, 95, 123, and 153 Ω for the reference sample and composites A, B, C, and D, respectively. Equivalent electrical circuit models have been adapted to Nyquist curves to simulate the corrosion resistance of composites. Three different circuit models were suggested and then employed to assess the EIS results (Fig. 8 and Table 3). The reference sample and composite A had a dissimilar equivalent circuit model compared to composites B, C, and D, as shown in Fig. 8. On the other hand, all composites had L_1 and R_1 circuit components representing the electrolyte behavior. L_1 represents electrolyte conductivity, while R_1 is attributed to electrolyte resistance. Furthermore, the common R_2 and C_1 symbolize the resistance and capacitance of the surface film.

Meanwhile, the R_3 and Q_1/Q_3 denote the surface heterogeneity's resistance and constant phase element. It should be noted that the combination of inductor L_4 and resistance element R_4 was added to express the products of

TABLE 4. The Data Extracted from Nyquist Plots in Fig. 8

Sample	L_1, H	R_1, Ω	C_1, F	R_2, Ω	Q_3, F.s^(–0.2)	R_3, Ω
*Reference						
Composite A	–8.43E-06	19.71	2.27E-03	10.1	–2.23E-3	62.02
Composite B	–1.44E-05	28.47	4.19E-06	67.01	12.05E-6	74.41
Composite C	1.99E-06	19.81	3.45E-08	105	41.76E-6	14.94
Composite D	–1.81E-05	47.89	5.92E-06	96.74	–0.181E-3	12.34

Sample	C_4, F	L_4, H	R_4, Ω	C_5, F	R_5, Ω
*Reference					
Composite A	9.05E-06	–	13.2	–	–
Composite B	–	442.1	112.8	5.36E-06	21.08
Composite C	–	495.2	265.3	5.11E-06	33.55
Composite D	–	679.4	156.8	6.21E-06	61.51

*L_1 = –68.86E-6 H, R_1 = 12.63 Ω, Q_1 = 0.20E-3 F.s^(-0.3), R_2 = 89.74 Ω, C_2 = 1.33E-9 F, R_3 = –92.4 Ω, L_4 = = 0.087 H, R_4 = 3.78 Ω, C_5 = –2.07E-6 F, R_5 = 51.86 Ω.

corrosion formed on the surface. For composite A, the last circuits R_4 and C_4 related to the resistance and capacitance of the film formed inside the pores. On the other hand, the composites B, C, and D had the circuits R_5 and C_5, representing the film's resistance and capacitance as composite A.

Data extracted from the equivalent electric circuit in Table 4 show that the resistance of the oxide film (interface solution/electrode) was higher for composite D with $R_2 = 96.74\ \Omega$ compared to other samples. This finding indicates that the protective corrosion film formed on the composite was more resistant to the attack of chloride (Cl^-) ions. Meanwhile, the second film generated by the pores was relatively poor for composite A with $R_4 = 13.2\ \Omega$. Conversely, composite D demonstrated the highest film resistance with $R_5 = 61.51\ \Omega$. Obviously, increasing the amount of Sr in the composite Mg–1Ca–1Y made the oxide film more resistant, increasing, thus, the corrosion resistance. Regarding the low-frequency branch, the L_4 value calculated from the inductive loop of reference composites, as well as composites B, C, and D, confirmed a reduction of ion transfer and was more pronounced for composite D.

CONCLUSIONS

In this work, the effect of adding strontium elements in the amount of 0.5, 1.0, 1.5, and 2.0 wt.% on the microstructure and corrosion properties of the new Mg–1Ca–1Y composite for biomedical implant applications was investigated.

The microstructure analysis showed that the mechanical milling alloying process successfully manufactured the new composite.

The phase analysis confirmed the formation of intermetallic phases Mg_2Ca, $Mg_{17}Sr_2$, and $Mg_{24}Y_5$. The corrosion potential and corrosion rate of composite D were more anodic than other composites, and the addition of Sr shifted it towards an anodic direction.

Passivation was observed for all samples, and the pit initiation was more positive for the reference composite. On the other hand, the corrosion resistance of the film was found more protective for composite D, followed by composite C, B, A, and reference samples.

In general, the findings demonstrate that the Sr element most probably participates in forming a protective oxide layer and decreases the galvanic effect in the Mg–1Ca–1Y composite. The Mg–1Ca–1Y–2Sr composite, newly developed by mechanical alloying, can be a good candidate for manufacturing biodegradable implants.

ACKNOWLEDGMENTS

This study was funded by Eskişehir Osmangazi University Scientific Research Projects Coordination Unit. Project Number: 2017-1624.

REFERENCES

1. M.P. Staiger, A.M. Pietak, J. Huadmai, and G. Dias, "Magnesium and its alloys as orthopedic biomaterials: A review," *Biomater,* **27**, No. 9, 1728–1734 (2006).
2. Y. Liu, B. Lu, and Z. Cai, "Recent progress on Mg- and Zn-based alloys for biodegradable vascular stent applications*, J. Nanomater*., 1310792 (2019).
3. Y. Li, L. Wang, S. Chen, D. Yu, W. Sun, and S. Xin, "Biodegradable magnesium alloy stents as a treatment for vein graft restenosis," *Yonsei Med. J.*, **60**, No. 5, 429–439 (2019).
4. S. Agarwal, J. Curtin, B. Duffy, and S. Jaiswal, "Biodegradable magnesium alloys for orthopaedic applications: A review on corrosion, biocompatibility and surface modifications," *Mater. Sci. Eng. C*, **68**, 948–963 (2016).
5. Y. Li, C. Wen, D. Mushahary, R. Sravanthi, N. Harishankar, G. Pande, and P. Hodgson, "Mg–Zr–Sr alloys as biodegradable implant materials*," Acta Biomater.*, **8**, No. 8, 3177–3188 (2012).
6. S.-H. Byun, H.-K. Lim, K.-H. Cheon, S.-M. Lee, H.-E. Kim, and J.-H. Lee, "Biodegradable magnesium alloy (WE43) in bone-fixation plate and screw*," J. Biomed. Mater. Research. Part B: Appl. Biomater.*, **108**, No. 6, 2505–2512 (2020).

7. G. Song and S. Song, "A possible biodegradable magnesium implant material," *Adv. Eng. Mater.*, **9**, No. 4, 298–302 (2007).
8. Y.F. Zheng, X.N. Gu, and F. Witte, "Biodegradable metals*,"* *Mater. Sci. Eng.: R: Reports*, **77**, 1–34 (2014).
9. Jing-feng Wang, Yao Ma, Shengfeng Guo, Weiyan Jiang, Qingshan Liu, "Effect of Sr on the microstructure and biodegradable behavior of Mg–Zn–Ca-Mn alloys for implant application," *Mater. Design.*, **153 (**2018). DOI:10.1016/j.matdes.2018.04.062.
10. Li Yan, Jiaxing Zhou, Zhenzhou Sun, Meng Yang, and Liqun Ma. Microstructure and bio-corrosion behaviour of Mg–5Zn–0.5Ca–*x*Sr alloys as potential biodegradable implant materials*. Mater. Research Exp*. **5**, No. 4 (2018).
11. H. Zengin, "Role of Sr in microstructure, hardness and biodegradable behavior of cast Mg–2Zn–2Ca–0.5Mn (ZXM220) alloy for potential implant application," *Int. J. Metalcasting* (2019).
12. Z. Li, M. Chen, W. Li, H. Zheng, C. You, D. Liu, F. Jin, "The synergistic effect of trace Sr and Zr on the microstructure and properties of a biodegradable Mg–Zn–Zr–Sr alloy*," J. Alloys Compd*., **702**, 290–302. (2017).
13. Y. Li, M. Li, W. Hu, P. Hodgson, and C. Wen, "Biodegradable Mg–Ca and Mg–Ca–Y alloys for regenerative medicine," *Mater. Sci. Forum*, **654–656**, 2192–2195 (2010).
14. Y.C. Li, C.S. Wong, C. Wen, and P.D. Hodgson, "Biodegradable Mg–Zr–Ca alloys for bone implant materials," *Mater. Technol*., **27**, No. 1, 49–51 (2012).
15. J. Wang, Y. Zhou, Z. Yang, S. Zhu, L. Wang, and S. Guan, "Processing and properties of magnesium alloy micro-tubes for biodegradable vascular stents," *Mater. Sci. Eng, C*, **90**, 504–513 (2018).
16. I.S. Berglund, H.S. Brar, N. Dolgova, A.P. Acharya, B.G. Keselowsky, M. Sarntinoranont, and M.V. Manuel, "Synthesis and characterization of Mg–Ca–Sr alloys for biodegradable orthopedic implant applications," *J. Biomed. Mater. Res. B. Appl. Biomater.*, **100**, No. 6, 1524–1534 (2012).
17. Z. Li, X. Gu, S. Lou, and Y. Zheng, "The development of binary Mg–Ca alloys for use as biodegradable materials within bone," *Biomater*., **29**, No. 10, 1329–1344 (2008).
18. J.C. Gao, S. Wu, Y. Wang, and L.Y. Qiao, "Study on corrosion and degradation behavior of Mg–Ca alloy in simulated body fluid," *Mater. Sci. Forum*, **610–613**, 942–945 (2009).
19. H.R.B. Rad, M.H. Idris, M.R.A. Kadir, and S. Farahany, "Microstructure analysis and corrosion behavior of biodegradable Mg–Ca implant alloys," *Mater. Design*, **33**, 88–97 (2012).
20. A. Incesu and A. Gungor, "Biocorrosion and mechanical properties of ZXM100 and ZXM120 magnesium alloys," *Int. J. Metalcast*., **13** (2019).
21. M.Ö. Öteyaka, *Influence of Ca and Sr Additions on Corrosion Behaviour in Aqueous Media of AZ and ZA Magnesium Alloys*, Laval University (Quebec, Canada), 2002.
22. M.Ö. Öteyaka, E. Ghali, and R. Tremblay, "Corrosion behaviour of AZ and ZA magnesium alloys in alkaline chloride media," *International Journal of Corrosion*, 1–10 (2012). doi:10.1155/2012/452631.
23. Y. Li, P.D. Hodgson, and C.E. Wen, "The effects of calcium and yttrium additions on the microstructure, mechanical properties and biocompatibility of biodegradable magnesium alloys," *J. Mater. Sci*., **46**, No. 2, 365–371 (2011).
24. Y.-C. Liu, D.-B. Liu, Y. Zhao, and M.-F. Chen, "Corrosion degradation behavior of Mg–Ca alloy with high Ca content in SBF," *Trans. Nonferrous Met. Soc. China*, **25**, No. 10, 3339–3347 (2015).
25. A. Mohamed, A.M. El-Aziz, and H.-G. Breitinger, "Study of the degradation behavior and the biocompatibility of Mg–0.8Ca alloy for orthopedic implant applications*," J. Magnesium Alloys*, **7**, No. 2, 249–257 (2019).
26. Y. Ding, Y. Li, and C. Wen, "Effects of Mg17Sr2 phase on the bio-corrosion behavior of Mg–Zr–Sr alloys*," Adv. Eng. Mater.*, **18**, 259–268 (2016).
27. H. Lai, J. Li, J. Li, Y. Zhang, and Y. Xu, "Effects of Sr on the microstructure, mechanical properties and corrosion behavior of Mg–2Zn–*x*Sr alloys,". *J. Mater. Sci*.: *Mater. Medicine*, **29**, No. 6, 87 (2018).

28. M. Cheng, J. Chen, H. Yan, B. Su, Z. Yu, W. Xia, and X. Gong, "Effects of minor Sr addition on microstructure, mechanical and bio-corrosion properties of the Mg–5Zn based alloy system," *J. Alloys Compd.*, **691**, 95–102 (2017).
29. D. Jiang, Y. Dai, Y. Zhang, C. Liu, and K. Yu, "Effects of Strontium addition on microstructure, mechanical properties, corrosion properties and cytotoxicity of Mg–1Zn–1Mn alloy," *Mater. Research Exp.*, **6**, No. 5, 056556 (2019).
30. D.-T. Chou, D. Hong, P Saha., J. Ferrero, B. Lee, Z. Tan, Z. Dong, and P.N. Kumta, "In vitro and in vivo corrosion, cytocompatibility and mechanical properties of biodegradable Mg–Y–Ca–Zr alloys as implant materials,". *Acta Biomater*, **9**, No. 10, 8518–8533 (2013).
31. M.I. Jamesh, G. Wu, Y. Zhao, D.R. McKenzie, M.M.M. Bilek, and P.K. Chu, "Electrochemical corrosion behavior of biodegradable Mg–Y–RE and Mg–Zn–Zr alloys in Ringer's solution and simulated body fluid," *Corros. Sci.*, **91**, 160–184 (2015).
32. S.A. Luffy, D.T. Chou, J. Waterman, P.D. Wearden, P.N. Kumta, and T.W. Gilbert, "Evaluation of magnesium-yttrium alloy as an extraluminal tracheal stent," *J. Biomed. Mater. Res. A*. **102**, No. 3, 611–620 (2014).
33. F. Zucchi, V. Grassi, A. Frignani, C. Monticelli, and G. Trabanelli, "Electrochemical behaviour of a magnesium alloy containing rare earth elements," *J. Appl. Electroch.*, **36**, No. 2, 195–204 (2006).
34. Dhyah Annur, A Suhardi, M. I. Amal, Mochammad Syaiful Anwar, and Ika Kartika, "Powder metallurgy preparation of Mg–Ca alloy for biodegradable implant application," *J. Physics: Conf. Series*, **817** (2017). DOI:10.1088/1742-6596/817/1/012062.
35. Z. Hussain, N. MohdIsa, B.K. Dhindaw, "Effect of alloying elements on properties of biodegradable magnesium composite for implant application," *J. Powder Metall. Min.*, **6**, 179 (2017).
36. M.M. Avedesian and H. Baker, *ASM Specialty Handbook: Magnesium and Magnesium Alloys*. ASM International (1999).
37. K.U. Kainer, *Magnesium: Proceedings of the 6th International Conference – Magnesium Alloys and Their Applications*. Wiley (2006).
38. R.D. Klassen, P.R. Roberge, A.M. Lafront, M.Ö. Öteyaka, and E. Ghali, "Corrosion behaviour of zinc and aluminum magnesium alloys by scanning reference electrode technique (SRET) and electrochemical noise (EN)," *Canad. Metall. Quarterly*, **44**, No. 1, 47–52 (2005).
39. M.Ö. Öteyaka, E. Ghali, and R. Tremblay, "Corrosion behaviour of AZ and ZA Magnesium alloys in alkaline chloride media," *Int. J. Corros*. (2012). https://doi.org/10.1155/2012/452631.